Maximum Likelihood Estimation of Synchronous Machine Parameters from Flux Decay Data

Adina Tumageanian, *Member, IEEE,* Ali Keyhani, *Senior Member, IEEE,*
Seung-Ill Moon, *Member, IEEE,* Thomas I. Leksan, *Member, IEEE,* and Longya Xu

***Abstract*— A time-domain system identification procedure to estimate the parameters of a 5 kVA salient pole synchronous machine from standstill test measurements is proposed. The test consists of a dc flux decay signal applied to the d-axis and q-axis of the machine. From the recorded responses to this signal, the admittance transfer function models and the SSFR equivalent circuit models are identified. The Maximum Likelihood algorithm is used to estimate the model parameter values, and the Akaike Criterion is used to select the best-fit model. The performance of the standstill models in the dynamic environment is studied through simulation of an on-line small-disturbance test. The results are compared with measured data.**

I. Introduction

STANDSTILL frequency response (SSFR) data and time domain response data are used for synchronous machine modeling and parameter estimation [1–9]. The SSFR test is a well-established procedure generally performed at very low flux levels, in the range of about 0.2% of the machine rating [6]. Additionally, the SSFR test requires fairly sophisticated equipment to minimize the levels of noise present especially in the low-frequency range. The results of the Standstill Frequency Response technique show that the estimated models are sufficiently accurate in the 0.1–10 Hz frequency range [7, 8].

Time domain methods have attracted attention due to the relatively simple testing procedures involved. In this paper, the machine is identified directly from time-domain standstill test data. A flux decay signal, in the range of 15% of the machine rating, is applied to the d- and q-axis of the machine. A stronger excitation of the machine field and damper circuit modes is thus available. The parameters of the admittance transfer function models and the equivalent circuit models are estimated from this data. The best-fit model from each model set is then selected based on the Akaike Criterion and physical reasoning. Lastly, the estimated model performance is evaluated using standstill and small-disturbance measured data.

Paper IPCSD 93–28, approved by the Electric Machines Committee of the IEEE Industry Applications Society and presented at the 1992 Industry Applications Society Annual Meeting, Houston, TX. Manuscript approved for publication June 2, 1993. This work was supported by the National Science Foundation under Projects ECS-9015773 and ECS-9204567.

A. Tumageanian is with General Electric Company, Schenectady, NY 12345 USA.

A. Keyhani and L. Xu are with the Department of Electrical Engineering at the Ohio State University, Columbus, OH 43210 USA.

S. I. Moon is with Chonbuk National University, Chongu, Republic of Korea.

T. Leksan is with Power Technologies, Inc., Roseville, CA 95661 USA.

IEEE Log Number 9216412.

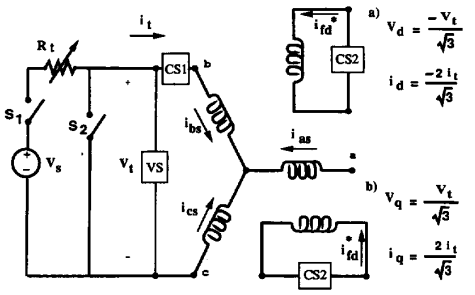

Fig. 1. Connection diagram for the d-q axis dc flux decay test.

II. Standstill Flux Decay Testing

The standstill test configuration is shown in Fig. 1. The setup is similar to that described in [6]. A three-phase salient-pole laboratory machine rated 5 kVA and 240 V is tested. A 12 V car battery is used as the input voltage source. The rheostat is used to adjust the input voltage until current less than the machine rating flows in the stator. When switch S_1 is closed, current is supplied to the machine and when S_2 is closed, the flux decay response is initiated. Simultaneously, the data acquisition system is triggered. The current sensors (CS1 and CS2) and voltage sensor (VS) record $v_s(t)$, $i_s(t)$, and $i_{fd}^*(t)$. * denotes the value on the field side, as measured with the machine in the d-axis position. Maximum coupling between the stator and field windings occurs in this position. Minimum coupling exists in the q-axis position. Using Park's transformation, the d-q axis data are obtained from the measured stator quantities (Fig. 1). For estimation purposes, a 0.8 second input-output history is recorded.

The concern in adjusting the dc armature current as described above is to avoid saturating the machine at standstill, and generally, current levels below 25% of the machine rms rating will achieve this goal. However, for small machines, the lower limit of measurable current is dictated by the sensitivity of the metering equipment used. For large machines, the dc current that can be supplied is limited by the size of the available dc source. For example in [2], the experimenters were able to use currents of approximately 125 A and 190 A for the 1100 MW and 600 MW machines, respectively.

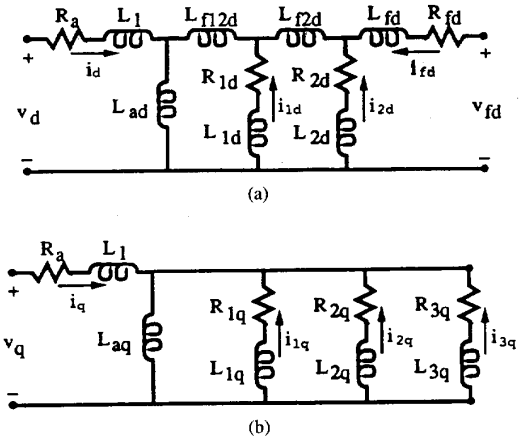

Fig. 2. SSFR3 circuit models. (a) d-axis model. (b) q-axis model.

III. Synchronous Machine Models

The synchronous machine can be represented by the Standard, SSFR2, and SSFR3 models. The SSFR3 model is shown in Fig. 2. The Standard, SSFR2 and SSFR3 differ in the number of damper windings and leakage inductances that they incorporate.

These models are based on the reciprocal per unit system in which all parameters are referred to the stator. In this study, the field winding current is measured on the field side and is referred to the stator using the equivalent turns ratio, a, between the field and stator:

$$i_{fd} = \frac{2}{3} \cdot a \cdot i^*_{fd}. \tag{1}$$

The field winding resistance value is also referred to the stator side as

$$R_{fd} = \frac{3}{2}\left(\frac{R^*_{fd}}{a^2}\right). \tag{2}$$

The discrete-time representation of the d-axis model of Fig. 2 is written as

$$X(k+1) = A_d \cdot X(k) + B_d \cdot U(k) + w(k) \tag{3}$$

$$Y(k+1) = C_d \cdot X(k+1) + v(k+1) \tag{4}$$

$$U = [v_d] \quad Y = [i_d\ i^*_{fd}]^T \quad X = [i_d\ i^*_{fd}\ i_{1d}\ i_{2d}]^T \tag{5}$$

$w(\cdot)$ and $v(\cdot)$ denote the process and measurement noise, respectively, and T denotes the transpose of the vector. The SSFR3 model parameter vector is

$$\theta_d = [R_a\ R^*_{fd}\ R_{1d}\ R_{2d}\ L_l\ L_{\rm ad}\ L_{fd}\ L_{1d}\ L_{2d}\ L_{f12d}\ L_{f2d}\ a] \tag{6}$$

in which L_{fd} is a stator referred value and the equivalent turns ratio, a, is a parameter to be estimated. The q-axis model of Fig. 2 is similarly modeled.

The computations of the A and B matrices from the continuous time-domain representation are described in [10]. The explicit parameterization of continuous system representation is given in [1].

In this study, voltage is the input signal and current is the output signal. Therefore, the transfer functions are in the form of admittances. With the field winding short-circuited, these transfer functions can be given as

$$\left.\frac{i_d(s)}{v_d(s)}\right|_{v^*_{fd}=0} = \frac{1}{R_a + sL_d(s)} \tag{7}$$

$$\frac{i_q(s)}{v_q(s)} = \frac{1}{R_a + sL_q(s)}. \tag{8}$$

The order of the transfer function is determined by the number of poles in the above equations. The third order d-axis transfer function model can be expressed as

$$\left.\frac{i_d(s)}{v_d(s)}\right|_{v^*_{fd}=0} = \frac{1}{R_a + s(L_\ell + L_{\rm ad})\frac{(1+T'_d s)(1+T''_d s)}{(1+T'_{\rm do} s)(1+T''_{\rm do} s)}}$$

$$= \frac{K(1+T'_{\rm do}s)(1+T''_{\rm do}s)}{(1+T_{d1}s)(1+T_{d2}s)(1+T_{d3}s)}. \tag{9}$$

The relationships between the coefficients of (9) and (10) is quite involved. However, if it is assumed that R_a is very small, then T_{d1} will be the longest time constant, related to R_a and L_d. Furthermore, the values of T_{d2} and T_{d3} will approach T'_d and T''_d, respectively.

IV. Maximum Likelihood Estimation

The Maximum Likelihood (ML) estimation method is used for synchronous machine model identification. The objective of ML identification is to estimate the parameter vector θ which maximizes the likelihood function, L(θ). The likelihood function is a conditional probability density function defined as [11]

$$L(\theta) = \prod_{k=1}^{N}\left[\frac{1}{\sqrt{(2\pi)^m \det(R(k))}} \exp\left(-\frac{1}{2}e^T(k)R^{-1}(k)e(k)\right)\right] \tag{10}$$

where $e(\cdot)$, $R(\cdot)$, N, and m denote the estimation error, the covariance of estimation error, the number of data points, and the dimension of the output Y, respectively. The covariance of the estimation error, $R(k)$, is defined as

$$R(k) = E\left[e(k) \cdot e(k)^T\right] \tag{11}$$

$$e(k) = Y(k) - \hat{Y}(k) \tag{12}$$

where $e(k)$ is the estimation error, $Y(k)$ is the measured output and $\hat{Y}(k)$ is the estimated output. Maximizing $L(\theta)$ is equivalent to minimizing its negative log function, defined as

$$V(\theta) = -\log L(\theta). \tag{13}$$

The parameter vector θ is computed iteratively using Newton's approach, and the cost function $V(\theta)$ is calculated at each iteration step. Therefore, $\hat{Y}$(k) must be determined at each step. The dynamic states involved, $X(k)$, are updated using Kalman filter theory [11].

V. The Akaike Information Criterion

As the number of parameters in a model increases, the cost function $V(\theta)$ will decrease or remain constant. However, as the complexity of a model increases, better initial parameters are needed for convergence of the ML algorithm. If an overfitted model is used, that is, one of higher order than the system under test, the ML estimation algorithm will again encounter numerical stability problems.

Therefore, to select the most suitable model, the model which has 1) the lowest cost function $V(\theta)$ and 2) the lowest order or smallest number of parameters is chosen. However, $V(\theta)$ may decrease as the model order or the number of parameters increases. As a result, this method may select an overfitted model. To avoid this problem, the Akaike Information Criterion (AIC) is used [12]. The AIC is defined as

$$\mathrm{AIC}(\hat{\theta}) = -2 * \log L(\hat{\theta}) + 2 * \mathrm{np} \tag{14}$$

where $\hat{\theta}$ is the estimated parameter vector and np is the number of parameters. The model with the minimum AIC value is generally selected as the best model. Thus, the cost function and AIC values are numerical tools which, along with physical reasoning, allow selection of the most suitable machine model.

VI. *D*-Axis Transfer Function Model Estimation

A parameter initialization technique must be used that will allow convergence of the ML algorithm to a realistic parameter set. To obtain the initial parameter value of the synchronous inductance, the machine open-circuit and short-circuit test data provided by the manufacturer can be used [13]. L_d is determined to be equal to 0.042 H. The initial value of R_a is calculated as 0.418 Ω from the d-axis flux decay steady-state data.

The graphical technique [4, 14] is used to estimate the machine time constants. This technique was originally proposed by deMello for machine parameter estimation using the response due to load rejection tests. However, the procedure herein discussed makes use of the standstill flux decay data, and the graphical procedure is applied to this data to determine the time constant values.

Three time constants (T_{d1}, T_{d2}, T_{d3}) are determined from the graphical method, and the third order transfer function is used to model the response. Thus, the initial values of $T_d^{'}$ and $T_d^{''}$ are obtained. $T_{\mathrm{do}}^{'}$ and $T_{\mathrm{do}}^{''}$ are initialized arbitrarily as five times $T_d^{'}$ and $T_d^{''}$, respectively. With the initialization complete, the ML method is applied. It is not known, however, if the third order transfer function best represents the measured response. Therefore, the second through fifth order transfer functions are estimated. Results for the third and fourth order models are given in Table I.

To obtain the initial values of the higher order models, the successive initialization technique is used where the estimated parameters of the lower order model are used as initial values for the next higher order model. The remaining parameters are initialized arbitrarily.

The AIC is used to determine the best fit model as the fourth order model, since it has the minimum value of AIC. The fifth order model shows no improvement in the cost function or the AIC value and is not shown in Table I.

TABLE I
D-Axis Transfer Function Model Parameter Estimation

	3rd Order		4th Order	
	Initial	Estimated	Initial	Estimated
R_a (Ω)	0.4180	0.4181	0.4181	0.4180
L_d (H)	0.0420	0.0368	0.0368	0.0372
$T_d^{'}$ (sec)	0.0747	0.0706	0.0706	0.0751
$T_d^{''}$ (sec)	0.0073	0.0118	0.0118	0.0169
$T_d^{'''}$ (sec)	——	——	0.0050	0.0003
$T_{do}^{'}$ (sec)	0.3730	0.7321	0.7321	0.7474
$T_{do}^{''}$ (sec)	0.0370	0.0167	0.0167	0.0240
$T_{do}^{'''}$ (sec)	——	——	0.0050	0.0006
$V(\hat{\theta})$		-3214.8		-3223.2
AIC		-6417.5		-6430.3

VII. *D*-Axis Equivalent Circuit Model Estimation

The parameters of the equivalent circuit models are also estimated using the flux decay response data. The Standard, SSFR2, and SSFR3 models are considered. The initial parameter values of the Standard model are obtained from the short circuit and open circuit data, from direct measurement, and from equations developed by Krause [15] relating the time constants to the circuit model parameters. In particular, the field, armature and damper winding parameters, are initialized using equations cited in [14], Appendix 6C. L_ℓ is selected as 2% of the estimated value of L_d.

The value of R_a estimated for the third order d-axis transfer function is used as the initial circuit model value. Its value is fixed for the estimation. R_{fd}^* is obtained by directly measuring the resistance of the field winding with a digital multimeter. The ML estimation is performed and the results for the Standard model are given in Table II.

The Standard and SSFR2 models differ by one parameter, the leakage inductance L_{f12d}. Successive initialization and estimation of the SSFR2 parameters shows that this inductance is nearly zero; the SSFR2 model is therefore the same as the Standard model.

The estimated parameters of the Standard model armature and field windings (R_a, R_{fd}^*, L_l, L_{ad}, L_{fd}, a) are used as the initial values of the SSFR3 field and armature winding parameters. R_a and L_{ad} are fixed for the estimation. Since the SSFR3 rotor body circuit is different from that of the Standard model, the initial damper winding parameters must be recalculated using the relation between the SSFR3 circuit parameters and the fourth order time constants [15]. It is found that including L_{f2d} and L_{f12d} in the SSFR3 model leads to numerical problems, and therefore, these parameters are excluded from the estimation. Results are given in Table II.

From Table II it is seen that the Standard model has the lowest value of AIC. The SSFR3 model has a higher AIC value, which indicates that it is overfitted. Thus, the Standard model is selected as the most suitable d-axis equivalent circuit model.

TABLE II
D-AXIS CIRCUIT MODEL PARAMETER ESTIMATION

	Standard		SSFR3	
	Initial	Estimated	Initial	Estimated
R_a (Ω)	(0.4181)[a]	(0.4181)	(0.4181)	(0.4181)
R^*_{fd} (Ω)	52.24	58.37	58.37	58.33
R_{1d} (Ω)	0.4547	0.6512	0.4663	0.6662
R_{2d} (Ω)	——	——	9.380	34.99
L_ℓ (H)	0.0007	0.0001	0.0001	0.0001
L_{ad} (H)	0.0362	0.0365	(0.0365)	(0.0365)
L_{fd} (H)	0.0031	0.0040	0.0040	0.0041
L_{1d} (H)	0.0048	0.0064	0.0075	0.0067
L_{2d} (H)	——	——	0.0031	0.0050
a	34.12	38.08	38.08	38.04
$V(\hat{\theta})$		-12081.4		-12082.4
AIC		-24146.6		-24144.2

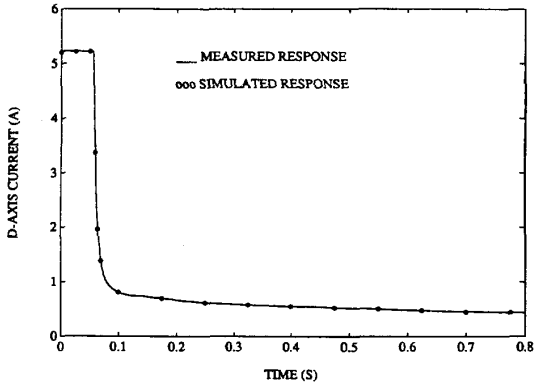

Fig. 3. Measured $i_d(t)$ response and simulated $i_d(t)$ response using the fourth order transfer function model.

VIII. *D*-AXIS MODEL STANDSTILL VALIDATION

In order to validate the models against the standstill flux decay response data, the measured and simulated output data are plotted together. It is found that the measured and simulated output data match very well for the time constant and circuit models discussed. For example, Fig. 3 shows the measured and simulated d-axis stator current $i_d(t)$ responses for the fourth order transfer function model. The Standard circuit model simulated response shows the same good fit.

IX. *Q*-AXIS TRANSFER FUNCTION MODEL ESTIMATION

The initial value of the armature inductance, L_q is not available. However, L_q is less than L_d for salient pole machines. Therefore, the initial value of L_q is selected as slightly less than the estimated value of L_d of the fourth order model. The initial value of R_a is obtained from the q-axis flux decay steady state data.

To obtain the initial values of the q-axis time constants, the graphical procedure is utilized with the standstill data for the machine in the q-axis position. Three time constants are calculated from the $i_q(t)$ response. With these initial values, the estimation of the third order model is performed.

TABLE III
Q-AXIS TRANSFER FUNCTION MODEL PARAMETER ESTIMATION

	3rd Order		4th Order	
	Initial	Estimated	Initial	Estimated
R_a (Ω)	0.4160	0.4162	0.4162	0.4160
L_q (H)	0.0350	0.0243	0.0243	0.0285
T'_q (sec)	0.1690	0.2705	0.2705	1.181
T''_q (sec)	0.0226	0.0164	0.0164	0.0253
T'''_q (sec)	——	——	0.0010	0.0069
T'_{qo} (sec)	0.8450	0.3357	0.3357	1.592
T''_{qo} (sec)	0.1130	0.0523	0.0523	0.0669
T'''_{qo} (sec)	——	——	0.0050	0.0101
$V(\hat{\theta})$		-3257.0		-3277.9
AIC		-6502.0		-6539.8

The successive initialization scheme is again utilized to initialize the parameters of the higher order transfer function models. The estimation of the transfer function models is performed and the results for the third and fourth order models are shown in Table III. It is found that the AIC values decrease up to the fifth order model, and if the AIC is strictly applied, the fifth order model should be chosen as the best fit model. However, the estimated value of L_q for the fifth order model is larger than the estimated value of L_d. This is not physically realizable. Therefore, the fourth order model is selected as the most suitable q-axis transfer function model.

X. *Q*-AXIS EQUIVALENT CIRCUIT MODEL ESTIMATION

The d-q axis models share two parameters, R_a and L_ℓ. The estimated d-axis values of R_a and L_ℓ are therefore used for the q-axis estimation. This reduces the number of parameters to be estimated by two. Since the Standard model was chosen as the best fit d-axis circuit model, the values of R_a and L_ℓ of this model are chosen and fixed for the estimation. L_{aq} is calculated by subtracting L_ℓ from L_q, estimated using the third order time constant model.

The initial values of the damper parameters are obtained by the method presented previously: relating the circuit parameters to the time constant values. With these initial estimates, the ML is employed. Results of the Standard model estimation are presented in Table IV.

For the SSFR3 model estimation, in addition to R_a and L_ℓ, L_{aq} is fixed to the value estimated for the Standard model. The damper windings are initialized as before. Results of the estimation are presented in Table IV. Note that the q-axis Standard and SSFR2 models are identical.

It is found that the SSFR3 model has a lower AIC value than the Standard model. However, it is not known if a model of higher order than the SSFR3 model is suitable. Therefore, the SSFR4 model, which has four rotor body circuits, is tested. It is found that this model is not physically realizable and has values of AIC and $V(\theta)$ that are higher than those of the SSFR3 model. The SSFR3 model is chosen as the most suitable equivalent circuit model.

XI. *Q*-AXIS MODEL STANDSTILL VALIDATION

The estimated q-axis models are verified by comparing their simulated q-axis stator current responses against the

TABLE IV
Q-AXIS CIRCUIT MODEL PARAMETER ESTIMATION

	Standard		SSFR3	
	Initial	Estimated	Initial	Estimated
R_a (Ω)	(0.4181)	(0.4181)	(0.4181)	(0.4181)
R_{1q} (Ω	0.3676	0.4177	0.0591	0.0401
R_{2q} (Ω)	0.5366	0.5341	0.4313	0.5994
R_{3q} (Ω)	——	——	2.114	2.829
L_ℓ (H)	(0.0001)	(0.0001)	(0.0001)	(0.0001)
L_{aq} (H)	0.0241	0.0244	(0.0244)	(0.0244)
L_{1q} (H)	0.0992	0.1170	0.0696	0.1402
L_{2q}(H)	0.0086	0.0087	0.0108	0.0132
L_{3q} (H)	——	——	0.0145	0.0168
$V(\hat{\theta})$		-3247.9		-3264.0
AIC		-6481.9		-6509.9

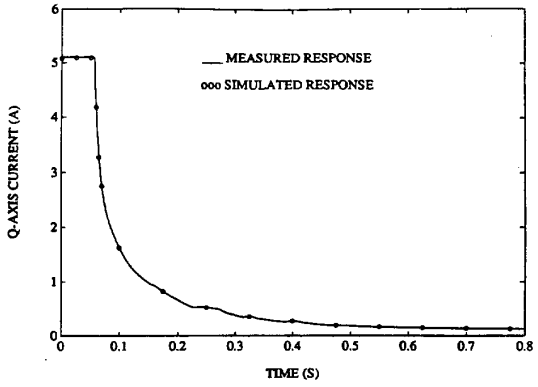

Fig. 4. Measured $i_q(t)$ response and simulated $i_q(t)$ response using the fourth order transfer function model.

measured standstill $i_q(t)$ response. For the best-fit q-axis transfer function and circuit models discussed above, it is again observed that the estimated model responses match the measured responses well. Fig. 4 shows the responses for the fourth order transfer function model.

XII. SMALL DISTURBANCE SIMULATION STUDY

To observe the dynamic behavior of the standstill estimated models, simulation of a small disturbance test is performed for the 240 V, 5 kVA machine. In the experiment, the machine is tied to the system bus through a tap-changing transformer. Using the tap, the voltage at the machine terminals is adjusted to approximately 170 V or 70% of its rating. The machine is therefore underexcited, and no significant saturation effects are present. The disturbance is achieved by changing the excitation reference voltage by 2% to 5% of the steady state value. The machine runs at minimal load.

The simulation is performed using the d-q axis Standard model with parameter values as listed in Tables II and IV. The inputs are the measured terminal voltage, in terms of V_d and V_q, and the field voltage. The simulated outputs are the armature current, in terms of i_d and i_q, and the field current on the rotor side, i^*_{fd}. The speed is assumed constant at rated value.

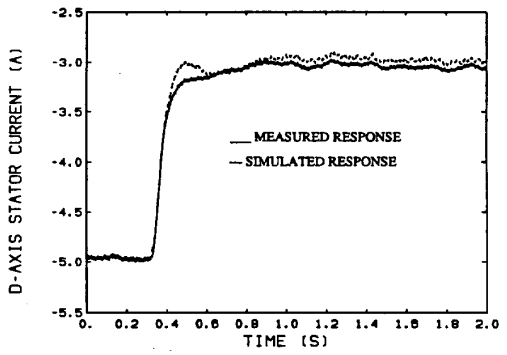

Fig. 5. The measured and simulated i_d(t) for the small disturbance test.

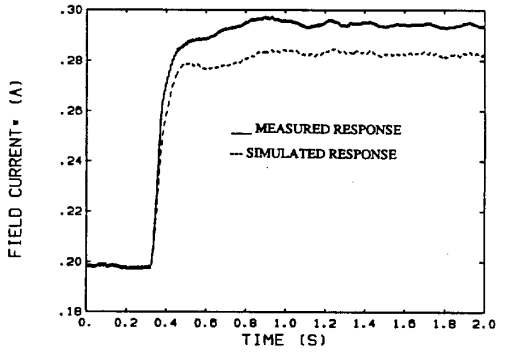

Fig. 6. The measured and simulated field current on the rotor side, i^*_{fd}(t), for the small disturbance test.

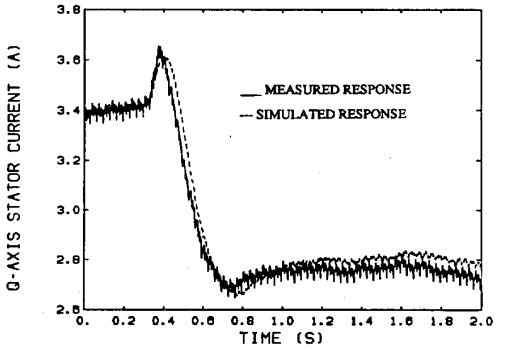

Fig. 7. The measured and simulated i_q(t) for the small disturbance test.

The simulation is performed, and it is observed that the simulated outputs generally follow the transient characteristics of the machine. Therefore, the model exhibits good dynamic behavior. However, a steady state error exists between the simulated and measured currents: approximately 7% for $i_d(t)$, 6% for $i_q(t)$, and 18% for $i^*_{fd}(t)$. For comparison purposes, Figs. 5, 6, and 7 show the measured and simulated responses without the steady-state error.

The results indicate that while the standstill time-domain data can be used to accurately model the machine at standstill, this data cannot provide sufficient dynamic information. For

example, on-line, the field resistance decreases due to the centrifugal forces which provide a tighter contact between the field supply terminals and the rotor. The damper resistance values may also decrease due to the rotational forces. Additionally, on-line, the d and q axes are no longer decoupled, as for the standstill condition. As a result, effects such as cross-magnetization, or the magnetic coupling between the d and q axes, will affect the on-line mutual inductance values, L_{ad} and L_{aq}. Rated on-line operation also entails slight saturation, which will also affect these parameter values. These phenomena physically cannot be represented by standstill machine data, in the time domain or frequency domain, and therefore cannot be reflected in the estimated parameters. Thus, the dynamic steady-state errors are observed in the simulated current responses.

XIII. Conclusion

This paper presents a step-by-step procedure to identify the model order, the model structure, and the linear parameter values of the d-q axis synchronous machine models using the standstill time-domain data. The flux decay test is performed on the 5 kVA salient pole synchronous machine. Physically realistic initial parameter values are computed based on the flux decay characteristics and the open/short circuit tests. The ML method is then able to converge to a unique set of parameters. Lastly, the Akaike Criterion is used to select the best-fit model structure.

This procedure yields standstill transfer function and equivalent circuit models which accurately simulate the machine dc flux decay response. It must be emphasized that the estimated linear parameters cannot directly represent the machine rated operating condition. However, the estimation procedure described in this paper is an important first step in determining the machine parameters, and the small disturbance test results verify the basic validity of the standstill model structures identified. The next step is to adjust the mutual inductance parameters based on saturation functions determined from several machine operating conditions.

References

[1] A. Keyhani, S. Hao and R. P. Schulz, "Maximum likelihood estimation of generator stability constants using SSFR test data," *IEEE Trans. Energy Conversion*, vol. 6, no. 1, pp. 140–154, March 1991.

[2] P. J. Turner, D. C. Macdonald and A. B. J. Reece, "The D. C. decay test for determining synchronous machine parameters: measurement and simulation," *IEEE Trans. Energy Conversion*, vol. 4, no. 4, pp. 616–623, Dec. 1989.

[3] P. J. Turner and D. C. Macdonald, "Transient electromagnetic analysis of the turbine generator flux decay test," *IEEE Trans. Power App. Syst.*, vol. PAS-101, no. 9, pp. 3193–3200, 1982.

[4] F. P. de Mello and J. R. Ribeiro, "Derivation of synchronous machine parameters from tests", *IEEE Trans. Power App. Syst.*, vol. PAS-96, no. 4, pp. 1211–1218, July/Aug. 1977.

[5] J. J. Sanchez-Gasca, C. J. Bridenbaugh, C. E. J. Bowler and J. S. Edmonds, "Trajectory sensitivity based identification of synchronous generator and excitation system parameters," *IEEE Trans. Power Syst.*, vol. 3, no. 4, pp. 1814–1822, Nov. 1988.

[6] E. S. Boje, J. C. Balda, R. G. Harley and R. C. Beck, "Time-domain identification of synchronous machine parameters from simple standstill tests," *IEEE Trans. Energy Conversion*, vol. 5, no. 1, pp. 164–170, March 1990.

[7] P. L. Dandeno and A. T. Poray, "Development of detailed turbogenerator equivalent circuits from standstill frequency response measurements," *IEEE Trans. Power App. Syst.*, vol. PAS-100, no. 4, pp. 1646–1655, April 1981.

[8] "IEEE standard procedure for obtaining synchronous machine parameters by standstill frequency response testing," *IEEE Std.* 115A–1987.

[9] L. X. Le and W. J. Wilson, "Synchronous machine parameter identification: a time domain approach," *IEEE Trans. Energy Conversion*, vol. 3, no. 2, pp. 241–248, June 1988.

[10] A. Keyhani and S. M. Miri, "Observers for tracking of synchronous machine parameters and detection of incipient faults," *IEEE Trans. Energy Conversion*, vol. EC-1, no. 2, pp. 184–190, June 1986.

[11] K. J. Åström, "Maximum likelihood and prediction error methods," *Automatica*, vol. 16, pp. 551–574, 1980.

[12] H. Akaike, "A new look at the statistical model identification", *IEEE Trans. Automat. Contr.*, vol. AC-19, no. 6, pp. 716–723, Dec. 1974.

[13] A. E. Fitzgerald, C. Kingsley, Jr. and S. D. Umans, *Electric Machinery*. New York: McGraw-Hill Book Company, 1983.

[14] "IEEE guide for synchronous generator modeling practices in stability analyses," *IEEE Std.* 1110–1991.

[15] P. C. Krause, *Analysis of Electric Machinery*. New York: McGraw-Hill Book Company, 1987.

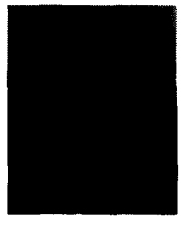

Adina Tumageanian (S'89–M'93) is a graduate of the Ohio State University, where she obtained the B.S. and M.S. degrees in Electrical Engineering in 1991 and 1993, respectively. As an undergraduate and graduate student she was elected into Tau Beta Pi and served as president of Eta Kappa Nu. She joined the General Electric Co. as a Design Engineer in May 1993, working in the Generator Development Group in Schenectady, NY.

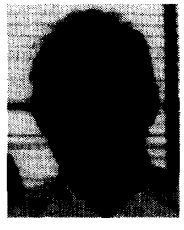

Ali Keyhani (S'72–M'76–SM'89) received the Ph.D. degree from Purdue University, West Lafayette, IN, in 1975. From 1967 to 1969 he worked for Hewlett-Packard Co. on the computer-aided design of electronic transformers. From 1970 to 1973 he worked for Columbus and Southern Ohio Electric Co. on computer applications for power system engineering problems. In 1974 he joined TRW Controls and worked on the development of computer programs for energy control centers. From 1976 to 1980 he was a Professor of Electrical Engineering at Tehran Polytechnic, Tehran, Iran. Currently Dr. Keyhani is a Professor of Electrical Engineering at The Ohio State University, Columbus, Ohio. His research interests are in control and modeling, parameter estimation, failure detection of electric machines, transformers and drive systems.

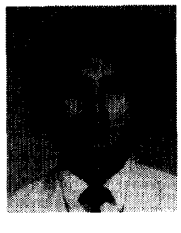

Seung-Ill Moon (S'90–M'92) received the B.S.E.E. degree from Seoul National University in 1985 and the M.S.E.E. and Ph.D. degrees from the Ohio State University in 1989 and 1993, respectively. Currently Dr. Moon is an Assistant Professor of Electrical Engineering at Chonbuk National University in the Republic of Korea.

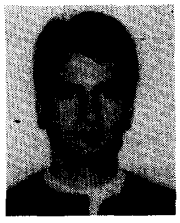

Thomas Leksan (S'88, M'91) received the B.S.E.E. degree from Cleveland State University in 1990 and the M.S.E.E. degree from the Ohio State University in 1991. He is presently an Analytical Engineer at Power Technologies, Inc., Roseville, CA, where he has performed studies dealing with the impact of windfarms on small systems and the use of battery energy storage as spinning reserve. He also has researched the effect of load characteristics on stabilizer tuning.

Longya Xu was born in Hunan, China. He graduated from the Shangtan Institute of Electrical Engineering in 1970. He received the B.S.E.E. degree from Hunan University in 1982 and the M.S. and Ph.D. degrees from the University of Wisconsin, Madison, in 1986 and 1990, respectively. Dr. Xu joined the Department of Electrical Engineering at the Ohio State University in 1990, where he is an Assistant Professor. His research and teaching interests include dynamic modeling and converter-optimized design of electrical machines and drive systems.